Research Article Vol. 30, No. 5 / 28 Feb 2022 / Optics Express 8212
Optics EXPRESS

Mechanism of brightness enhancement in multimode LD-pumped graded-index fiber Raman lasers: numerical modeling

OLEG S. SIDELNIKOV,[1,4] EVGENY V. PODIVILOV,[1,2] MIKHAIL P. FEDORUK,[1] ALEXEY G. KUZNETSOV,[2] STEFAN WABNITZ,[1,3] AND SERGEY A. BABIN[1,2,5]

[1]*Novosibirsk State University, 2 Pirogova str., Novosibirsk 630090, Russia*
[2]*Institute of Automation and Electrometry, SB RAS, 1 Ac. Koptyug ave., Novosibirsk 630090, Russia*
[3]*DIET, Sapienza University of Rome, Via Eudossiana 18, I- 00184 Rome, Italy*
[4]*o.sidelnikov@g.nsu.ru*
[5]*babin@iae.nsk.su*

Abstract: We develop a comprehensive theory for describing the experimental beam profiles from multimode fiber Raman lasers. We take into account the presence of random linear mode coupling, Kerr beam self-cleaning and intra-cavity spatial filtering. All of these factors play a decisive role in shaping the Stokes beam, which has a predominant fundamental mode content. Although the highly multimode pump beam is strongly depleted, it remains almost insensitive to the different physical effects. As a result, the intensity of the output Stokes beam is an order of magnitude higher than the pump intensity at its maximum, in quantitative agreement with the experimental results and in contrast with the simplified balance model.

1. Introduction

The Raman beam cleanup (RBC) effect was first experimentally demonstrated in 1979 by Andreev et al. [1], and it provided an effective solution for the improvement of both quality and brightness of high-power solid-state or excimer laser beams at their Raman conversion in gaseous [2] or solid-state [3] media. This idea was further applied to Raman lasers based on a multimode fiber, in which low-quality multimode pump radiation is converted into a high-quality Stokes beam [4]. A previous analysis of pump and Stokes modes overlap integrals [5] has shown that the RBC effect is present in graded-index fibers, where lower-order Stokes modes have higher Raman gain for random pump launching conditions. Whereas in step-index fibers all transverse modes have nearly the same Raman gain. The available analysis of small-signal gain remains only qualitative, and it is not applicable to multimode fiber Raman lasers [4], where pump-to-Stokes conversion occurs within the cavity, and a strong signal is generated.

Recently, high-power Raman lasers based on multimode graded-index (GRIN) fibers have attracted a great deal of attention [6–8]. Especially interesting is the opportunity of obtaining efficient Raman conversion of highly-multimode (M^2~30) radiation from high-power laser diodes (LDs) into a high-quality (M^2~2) Stokes beam. This was implemented in an all-fiber scheme including a in-fiber fiber Bragg grating (FBG) cavity and fiber coupling of the LD pump radiation, see [9] for a review. Using commercially available GRIN fibers and 9xx-nm LDs, such Raman lasers may generate high-quality radiation at wavelengths <1 μm, where emission by conventional singlemode Yb-doped fiber lasers is hardly possible. Connecting several high-power LDs to a GRIN fiber with 100-μm core through a multimode 100-μm fiber pump combiner, allows for increasing the coupled pump power up to 200 W in this scheme, and to generate Stokes radiation with output powers 50-60 W at wavelengths 954 [9] and 976 [10] nm by using 915 and 940 nm LDs, respectively. Herewith, the optimization of the transverse profile of FBGs

#449773 https://doi.org/10.1364/OE.449773
Journal © 2022 Received 29 Nov 2021; revised 16 Jan 2022; accepted 21 Jan 2022; published 25 Feb 2022

Optics EXPRESS

inscribed by femtosecond point-by-point technique in the near-axis part of the GRIN core enables a stronger spatial filtering effect, and it allows for improving the Stokes beam quality to $M^2<2$ almost without any loss of the conversion efficiency, thus providing a pump-to-Stokes brightness enhancement factor of >70 [10]. Besides, measurements of output beam profiles [10] show a strong depletion of the pump beam, with burning of a hole that is much broader than the Stokes beam profile. At the same time, simplified analytical models that were developed on the basis of radially-dependent balance equations [10] do not describe neither the beam profiles, nor the brightness enhancement which are observed in experiments.

This paper is an expanded version of Ref. [11]. Here we present in detail the results of numerical simulations of beams emerging from a multimode fiber Raman laser. The simulations are based on a comprehensive coupled-mode model, which takes into account both Raman and Kerr nonlinearity, random mode coupling and spatial filtering, for describing the propagation of pump and Stokes beams inside a GRIN fiber cavity. This permits us to successfully compare the theoretical predictions for beam profiles and intensities with the experimental observations.

2. Balance equations

We consider a GRIN fiber of 1 km length with the following refractive index profile:

$$n(r) = \begin{cases} n_0\sqrt{1-\Delta_\beta r^2} & r<a \\ n_{cl} & r \geq a \end{cases}, \tag{1}$$

where $n_0 = 1.47$ and $n_{cl} = 1.457$ are the refractive indices of the core and cladding, respectively, $a = 50\mu$m is the core radius, and $\Delta_\beta = \sqrt{2\Delta}/a$ is the mode spacing, where $\Delta = (n_0^2 - n_{cl}^2)/2n_0^2$. A pump wave with a wavelength of $\lambda_P = 940$ nm and a Stokes component with $\lambda_S = 976$ nm propagate simultaneously along the fiber. A pump wave with a parabolic intensity profile was applied to the fiber input, filling the entire fiber core. With increasing pump power, the power of the Stokes wave will also increase, which will lead to depletion of the pump. It is expected that, due to this pump depletion, a dip will be formed in the centre of the transverse distribution of the pump wave intensity, the radius of which will be equal to the radius of the fundamental mode.

To simulate the propagation of Stokes and pump waves through a multimode fiber, we first considered a model based on the balance equations [12]:

$$\frac{dI_s}{dz} = g_R k_S I_P I_s - \alpha_S I_s, \tag{2}$$

$$\frac{dI_P}{dz} = -g_R k_P \frac{\lambda_S}{\lambda_P} I_S I_P - \alpha_P I_P, \tag{3}$$

where I_P and I_S are the intensities of the pump wave and of the Stokes component, respectively, $\alpha_{S|P}$ are their loss factors, $k_{S|P} = 2\pi n_0/\lambda_{S|P}$ is the wavenumber, and g_R is the Raman gain estimated by the pump power threshold. A radial dependence of the intensities of all waves was assumed for this model, and the multipass problem was solved until a stable output distribution of the pump wave and the Stokes component was established. At each passage of the Stokes wave, 153-W of pump radiation was supplied to the fiber input. At the output, the Stokes component passed through a filter which reflected 4% of the power of the fundamental mode, and 0.4% of the power of each of the other modes, similar to the experimental conditions from [10].

Figure 1 shows the output distribution of the intensities of the pump wave and the Stokes component, as they are obtained by numerical solving the balance equations. One can see that the pump wave is depleted at the centre, and a large dip is formed in its distribution. This is due to the fact that the Stokes component has a small radius, and within the framework of this model, energy exchange occurs locally between the intensities of the Stokes wave and pump

Optics EXPRESS

wave, which have the same radial coordinates. Although the model qualitatively explains the dip formation, it does not properly describe the intensity of the generated Stokes wave. Indeed, in the frame of this model, the Stokes intensity cannot exceed the intensity of the undepleted pump wave. Therefore, we concluded that the model of Eqs. (2)–(3) is rather crude, since the interaction of the pump wave and the Stokes component does not occur pointwise (or locally), because the modes have a finite size. In addition, the balance equations do not allow the effects associated with the Kerr nonlinearity and random coupling of spatial modes to be described. On the other hand, experiments have shown that these effects can have a significant role in the Raman amplification of a Stokes wave by a pump wave in GRIN fibers [10], as well as for the propagation of a single beam [13,14]. Therefore, in order to properly describe the experiments, it is necessary to construct a more detailed coupled-mode model.

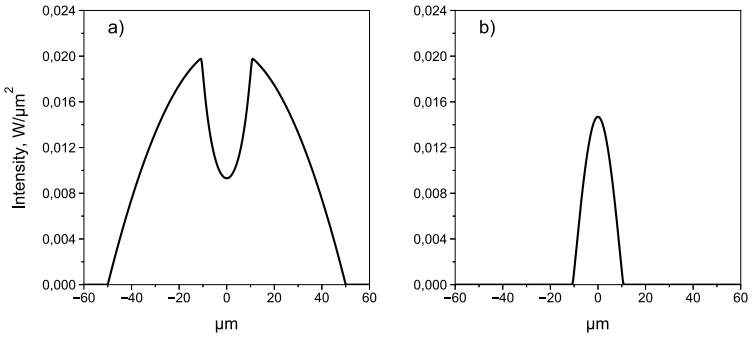

Fig. 1. Output distributions of the intensities of the pump wave (a) and the Stokes component (b), obtained using the balance equations.

3. Coupled-mode model

For a more accurate description of the process of propagation of the pump wave and the Stokes component in a multimode GRIN fiber, let us derive and investigate a system of equations based on a coupled-mode model. We introduce the following dimensionless and normalized variables:

$$\zeta = z\Delta_\beta, \quad \rho_{S,P} = 1/\sqrt{k_{S,P}\Delta_\beta}, \quad E^{S,P} = \Psi^{S,P}\sqrt{P^{S,P}}, \tag{4}$$

where E^S and E^P are the field envelopes of the Stokes and pump waves, respectively.

With this notation, the propagation of the pump wave and of the Stokes component in GRIN MMFs can be described by the coupled system of multidimensional nonlinear Schrödinger equations [12,15]:

$$\frac{d\Psi^S}{d\zeta} + i\frac{1}{2k_S\Delta_\beta}\frac{d^2\Psi^S}{dr^2} - i\frac{k_S}{2}\Delta_\beta r^2\Psi^S = -i\frac{k_S n_2}{\Delta_\beta n_0}\left(P^S\left|\Psi^S\right|^2 + P^P\left(2+if\right)\left|\Psi^P\right|^2\right)\Psi^S, \tag{5}$$

$$\frac{d\Psi^P}{d\zeta} + i\frac{1}{2k_P\Delta_\beta}\frac{d^2\Psi^P}{dr^2} - i\frac{k_P}{2}\Delta_\beta r^2\Psi^P = -i\frac{k_P n_2}{\Delta_\beta n_0}\left(P^P\left|\Psi^P\right|^2 + P^S\left(2-if\right)\left|\Psi^S\right|^2\right)\Psi^P, \tag{6}$$

where $f = 0.2$ is the ratio between the Raman and Kerr contributions. The complex field envelope in a GRIN fiber can be decomposed into a sum of Laguerre Gaussian (LG) modes, weighted by

Optics EXPRESS

the slowly varying mode amplitudes [16]:

$$\Psi^S(\zeta, r, \phi) = \sum_{m,p=0}^{\infty} A_{p,m}(\zeta) U^S_{p,m}(r, \phi), \tag{7}$$

$$\Psi^P(\zeta, r, \phi) = \sum_{m,p=0}^{\infty} B_{p,m}(\zeta) U^P_{p,m}(r, \phi), \tag{8}$$

where

$$U^{S,P}_{p,m}(r, \phi) = N_{p,m} \frac{r^{|m|}}{\rho^{|m|+1}_{S,P}} L^{|m|}_p \left(\frac{r^2}{\rho^2_{S,P}} \right) e^{\frac{-r^2}{2\rho^2_{S,P}}} e^{im\phi}. \tag{9}$$

Here $A_{p,m}$ and $B_{p,m}$ are the mode amplitudes of the Stokes and pump waves, respectively, p and m are radial and azimuthal mode orders, $L^{|m|}_p$ are Laguerre polynomials, and $N_{p,m}$ is a normalization coefficient. By substituting the decomposition (7) and (8) into Eqs. (5) and (6), using the orthonormality of the spatial distribution of the modes, and neglecting rapidly oscillating resonant four-wave mixing (FWM) terms, one obtains the coupled-mode model equations for the amplitudes of the pump wave and of the Stokes component in GRIN MMFs:

$$\begin{aligned} \frac{\partial A_{p,m}}{\partial z} = & \sum_{m1,p1} C^{p1,p}_{m1,m} A_{p1,m1} - \frac{\alpha_S}{2} A_{p,m} - \\ & - i \frac{k_S n_2}{\Delta_\beta n_0} \sum_{m1,m2,m3} \sum_{p1,p2,p3} q^{p1,p2,p3,p}_{m1,m2,m3,m} P^S A^*_{p1,m1} A_{p2,m2} A_{p3,m3} - \\ & - i \frac{k_S n_2}{\Delta_\beta n_0} g^{p1,p2,p3,p}_{m1,m2,m3,m} P^P (2 + if) B^*_{p1,m1} B_{p2,m2} A_{p3,m3}, \end{aligned} \tag{10}$$

$$\begin{aligned} \frac{\partial B_{p,m}}{\partial z} = & \sum_{m1,p1} C^{p1,p}_{m1,m} B_{p1,m1} - \frac{\alpha_S}{2} B_{p,m} - \\ & - i \frac{k_S n_2}{\Delta_\beta n_0} \sum_{m1,m2,m3} \sum_{p1,p2,p3} h^{p1,p2,p3,p}_{m1,m2,m3,m} P^S B^*_{p1,m1} B_{p2,m2} B_{p3,m3} - \\ & - i \frac{k_S n_2}{\Delta_\beta n_0} l^{p1,p2,p3,p}_{m1,m2,m3,m} P^P (2 + if) A^*_{p1,m1} A_{p2,m2} B_{p3,m3}, \end{aligned} \tag{11}$$

where

$$q^{p1,p2,p3,p}_{m1,m2,m3,m} = \int_0^{2\pi} d\phi \int_0^{\infty} r U^{S*}_{p1,m1} U^S_{p2,m2} U^S_{p2,m2} U^{S*}_{p,m} dr, \tag{12}$$

$$g^{p1,p2,p3,p}_{m1,m2,m3,m} = \int_0^{2\pi} d\phi \int_0^{\infty} r U^{P*}_{p1,m1} U^P_{p2,m2} U^S_{p2,m2} U^{S*}_{p,m} dr, \tag{13}$$

$$h^{p1,p2,p3,p}_{m1,m2,m3,m} = \int_0^{2\pi} d\phi \int_0^{\infty} r U^{P*}_{p1,m1} U^P_{p2,m2} U^P_{p2,m2} U^{*P}_{p,m} dr, \tag{14}$$

$$l^{p1,p2,p3,p}_{m1,m2,m3,m} = \int_0^{2\pi} d\phi \int_0^{\infty} r U^{S*}_{p1,m1} U^S_{p2,m2} U^P_{p2,m2} U^{P*}_{p,m} dr. \tag{15}$$

The obtained coupled-mode model allows one to simultaneously take into account the nonlinear effects of self- and cross-phase modulation, as well as stimulated Raman scattering. In addition to nonlinear effects, Eqs. (10)–(11) also take into account the presence of random linear coupling between all spatial modes, due to various fiber imperfections, bends and stresses, see [17] for

Optics EXPRESS

more details. We consider random coupling between all modes, and the coefficients $C^{p1,p}_{m1,m}(z)$ are normally distributed random numbers with zero mean and standard deviation s. Moreover, in order that linear mode coupling preserves the total beam power, it is necessary that the matrix C is Hermitian. Fiber losses for the Stokes ($\alpha_S = 2.64$ dB/km) and pump ($\alpha_S = 2.72$ dB/km) waves were also included in the model. In simulations, we consider 496 modes with mode number $n = 2p + |m| \leq 30$. This number of modes is justified by the fact that, on the one hand, it is enough to obtain the parabolic intensity profile observed in the experiments at the fiber output [10]. And on the other hand, we limit the number of considered modes in order to speed up the simulations.

It should be noted that Eqs. (10)–(11) do not describe the evolution of the full field, but separately the evolution of the amplitude of each mode of the Stokes $A_{p,m}$ and pump $B_{p,m}$ waves. This approach may significantly reduce the computation time, when compared with models based on the 3D nonlinear Schrödinger equation, owing to the use of a large integration step, which is permitted by neglecting rapidly oscillating FWM terms.

As the initial conditions for the Stokes wave, we used the decomposition of a Gaussian beam with a radius of 12 μm into spatial modes of the GRIN fiber; we also initially set a random input phase for each mode. For the pump wave, all modes have equal input intensities and random phases, in accordance with the parabolic profile observed in the experiment [10]. Calculations were performed for different realizations of the random phases, and then the results were averaged. The numerical simulation was performed for the scheme corresponding explicitly to the experimental one [10]. We also consider the multi-pass problem. For the first pass of the Stokes wave, the described Gaussian beam was used at the input. In order to match the physical experiment and for taking into account the FBG cavity, we added a 4% output coupler that filters the fundamental mode at the fiber output. Hence, after each pass, the amplitude of the fundamental mode of the Stokes wave was multiplied by $\sqrt{0.04}$ (this corresponds to the action of the filter after a round trip of propagation), and the other modes were multiplied by $\sqrt{0.004}$; the resulting beam was used as the input data for the next pass. For the pump wave, all modes were initialized with equal intensities and random phases at the input of each pass. Starting from the noise, the simulation with multiple passes of the Stokes wave through the resonator is performed, until it reaches a steady state in terms of Stokes power.

For the numerical solution of Eqs. (10)–(11), we wrote the system of equations in matrix form:

$$\frac{\partial A}{\partial z} = M_A A, \tag{16}$$

$$\frac{\partial B}{\partial z} = M_B B, \tag{17}$$

where A and B are vectors containing the amplitudes of all Stokes and pump modes, respectively; the matrices M_A and M_B correspond to the right-hand side of the coupled-mode model. If random linear coupling is neglected, the numerical solution can be calculated by using the following finite-difference scheme:

$$\frac{A^{n+1} - A^n}{h} = M^n_A A^n, \tag{18}$$

$$\frac{B^{n+1} - B^n}{h} = M^n_B B^n, \tag{19}$$

where A^n and B^n are the solution at the nth step, and h is the integration step. This numerical method has an accuracy of the second order $O(h^2)$, and it allows us to solve the equations with high precision. But when we take into account the presence of random linear coupling at each integration step, the numerical solution obtained by this method starts to diverge, due to the fact that the used finite-difference scheme does not conserve the Hamiltonian. In order to avoid this

Optics EXPRESS

numerical instability, we propose to use the following numerical scheme to solve the propagation Eqs. (10) and (11):

$$A^{n+1} = e^{hM_A^n} A^n, \tag{20}$$

$$B^{n+1} = e^{hM_B^n} B^n. \tag{21}$$

This scheme requires calculating the matrix exponent at each integration step, which is a time-consuming operation, but at the same time it allows us to preserve the total energy. To reduce the calculation time, the matrix exponent can be evaluated by using the Padé approximation [18]:

$$e^X \approx \left[\sum_{j=0}^{n} \frac{(2n-j)!n!}{(2n)!(n-j)!j!} X^j\right]^{-1} \sum_{j=0}^{n} \frac{(2n-j)!n!}{(2n)!(n-j)!j!} (-X)^j. \tag{22}$$

In the calculations, we used the expansion of the exponent up to the third term inclusive ($n = 3$).

4. Numerical results

Let us start our analysis from the Raman lasing threshold (P_{in} = 110 W). We consider beam propagation taking into account: (i) the Raman effect only, without fundamental mode filter (violet curves); (ii) Raman effect and random linear coupling without filter (red curves); (iii) Raman and Kerr effects, random linear coupling and FM filter (blue curves), see Fig. 2 with Stokes profiles normalized to 1 W power. In the case of considering only the Raman effect, after convergence, almost all of the energy of the Stokes component is contained in the fundamental mode of the GRIN MMF (99%). The mode content is determined by calculating the overlap integral of the output beam with the corresponding mode. When random linear coupling is included in the model, the FM content of the Stokes beam is nearly halved, with corresponding reduction of its peak intensity. Adding the Kerr effect leaves the profile almost unchanged due to the low Stokes intensity. Finally, inserting a spatial filter in the presence of random coupling increases the fundamental mode content, as well as the maximum Stokes beam intensity, but not up to its maximum possible value.

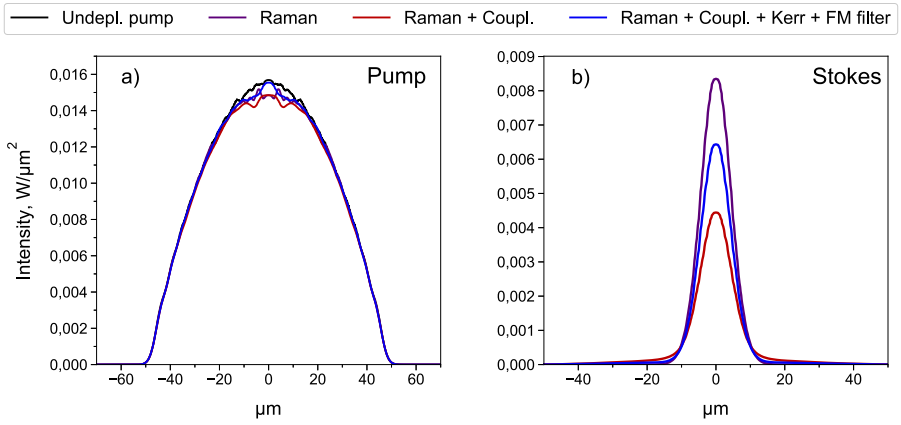

Fig. 2. Output spatial distributions of the intensities of the pump wave (a) and the Stokes component (b) for different propagation regimes near the Raman threshold.

As a next step, we consider Raman lasing well above threshold, where significant pump depletion occurs, and the Stokes wave becomes most intensive (P_{in} = 153 W). At first, let us

Optics EXPRESS

compare the profiles obtained with the balance equations (Fig. 1) with those from the coupled-mode model (10-11), were only terms corresponding to the Raman effect and fiber losses were retained. Figure 3 shows the output distributions of the intensities of the pump wave and the Stokes component, corresponding to the case of a 4% output coupler for all modes (red curves). The black curve corresponds to an undepleted pump beam, i.e., a replica of the input beam when just taking into account the presence of linear fiber attenuation. As we can see, in this case a large dip is obtained at the center of the spatial distribution of the pump wave intensity. In contrast to the balance equations (see Fig. 1), the boundaries of the dip are smoothed, in accordance with the finite sizes of the modes. Moreover, a clear mode structure with radial modulation of the intensity is seen both in the depleted pump dip and in the Stokes beam profiles, exhibiting a transverse substructure which is defined by the presence of high-order modes.

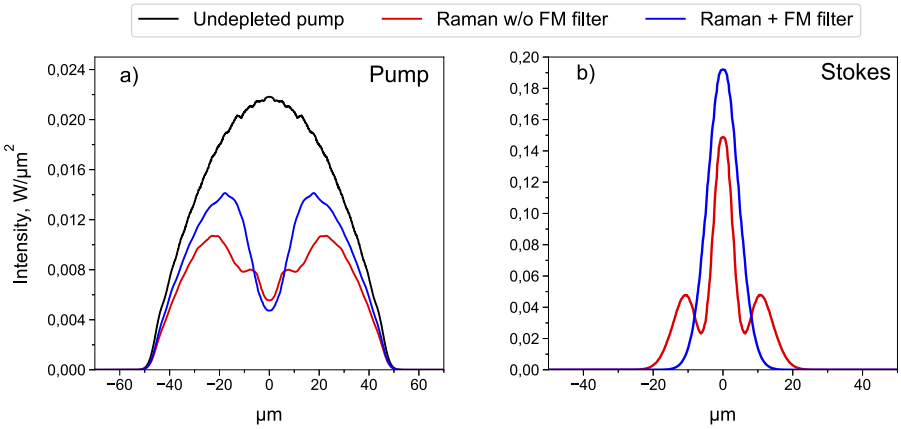

Fig. 3. Output spatial distributions of the intensities of the pump wave (a) and the Stokes component (b) for the coupled mode model, which takes into account only Raman effects and the losses in the fiber.

When we add the intra-cavity filter, suppressing high-order modes by 10 dB in comparison with the fundamental one, the output intensity profile of the Stokes component takes the form of a Gaussian distribution with predominant content of the fundamental mode (blue curves). Although the obtained spatial intensity distributions are in qualitative agreement with the results of the model based on balance equations, significant quantitative differences are observed, which are important for properly describing the experiment.

Adding random mode coupling for both beams in a non-filtering cavity (red curves in Fig. 4) washes out the modulation of the Stokes beam intensity, so that the dip in the depleted pump beam becomes broader, and it gets closer to the experimental results presented in [10]. However, one also obtains a smooth multimode Stokes beam, which is much broader than in the experiment. The inclusion of the Kerr effect (blue curves) permits us to significantly compress the width of the Stokes beam, by increasing the portion of energy contained in the fundamental mode. At the same time, the pump depletion becomes slightly deeper.

At last, adding spatial filtering of the fundamental mode (with 10 dB suppression of high-order modes) permits to significantly improve the Stokes beam quality, so that it becomes close to the experimental value (see Fig. 5(a)). In this case, almost all of the energy contained in HOMs is dissipated after each pass, so that the most of Stokes beam energy is confined in the fundamental mode (about 70%). In Fig. 5 we compare the simulation results with the experimental profiles [10] for input and output pump and generated Stokes beams. The comparison between experiments and simulations shows a very good agreement, both in the qualitative shapes of the beams, and in the quantitative intensity values.

Optics EXPRESS

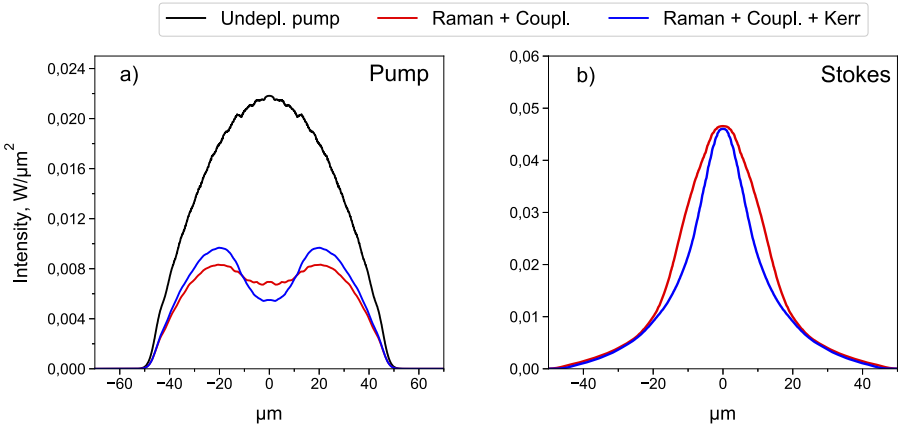

Fig. 4. Output spatial distributions of the intensities of the pump wave (a) and the Stokes component (b) for different propagation regimes above the Raman threshold.

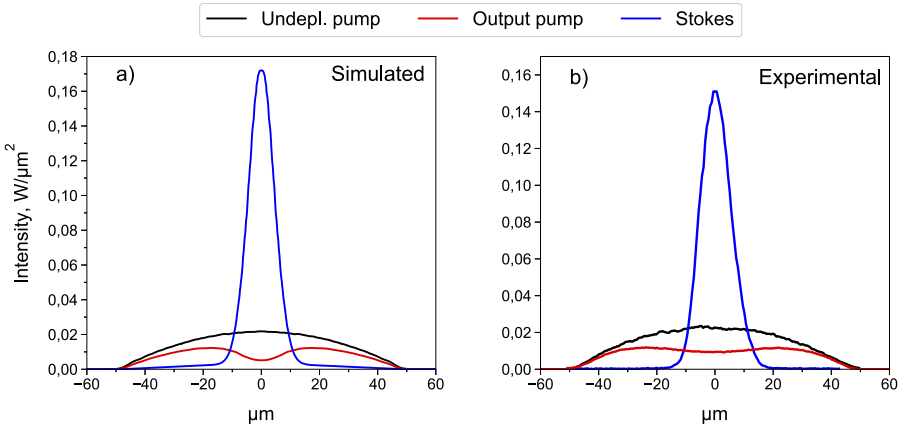

Fig. 5. Simulated (a) and experimental (b) profiles for the attenuated and depleted pump beam and corresponding Stokes beam, calculated with an account for the random mode coupling, Raman and Kerr nonlinearities, and spatial filtering effects.

To summarize, our simulations have revealed that random mode coupling greatly broadens and reduces the intensity of the Stokes beam, whereas Kerr self-cleaning and spatial filtering effects enhance both the beam quality and the peak intensity (by one order of magnitude, when compared with the pump intensity) of the Stokes wave. As a result, a high brightness enhancement factor in the process of pump-to-Stokes conversion is obtained. At the same time, the depleted pump beam profiles remain always weakly sensitive to the different physical effects.

5. Conclusion

In this work we studied by numerical simulations the propagation of Stokes and pump beams in a multimode GRIN fiber Raman laser. We introduced a system of equations based on the coupled-mode approach, including the presence of stimulated Raman scattering, the Kerr effect, fiber losses, intra-cavity spatial filtering and random linear mode coupling. Numerical results show that taking these effects into account leads to significant differences, as far as the intensity profiles of the pump and the Stokes beams are concerned, with respect to results obtained on the basis of a simple model, such as the balance equations, which only provides a qualitative picture.

Optics EXPRESS

Simulations based on our model are in very good quantitative agreement with experimental results [10]. Our approach can fully explain the pump-to-Stokes brightness enhancement, that can be achieved via the compensation of strong random mode coupling by spatial filtering and the Kerr effect. All of these factors are important for the Stokes wave, whereas they are basically irrelevant for shaping the highly multimode pump beam. Note that similar brightness enhancement can also be obtained in half-open cavities with random distributed feedback via Rayleigh backscattering, which also provides a mechanism of spatial filtering in multimode GRIN fibers [19].

Funding. European Research Council (740355); Ministry of Education and Science of the Russian Federation (14.Y26.31.0017, FSUS-2020-0034); Russian Foundation for Basic Research (18-52-7822); Russian Science Foundation (20-11-20040, 21-42-00019).

Acknowledgments. The work of M.P.F. (theoretical analysis) was supported by the Russian Science Foundation (Project No. 20-11-20040), the work of O.S.S. (mathematical modelling) was supported by the State Assignment for Fundamental Research (No. FSUS-2020-0034). The work of E.V.P., S.A.B. and S.W., related to the comparison of the adequacy of numerical models and their applicability for describing the experiment, was supported by the Ministry of Science and Higher Education of the Russian Federation (Project No. 14.Y26.31.0017) and Russian Foundation for Basic Research (grant 18-52-7822) together with the work of A.G.K. supported by Russian Science Foundation (grant 21-42-00019). S.W. was also supported by the European Research Council (grant no. 740355).

Disclosures. The authors declare no conflicts of interest.

Data availability. Data underlying the results presented in this paper are not publicly available at this time but may be obtained from the authors upon reasonable request.

References

1. N. F. Andreev, V. I. Bespalov, A. M. Kiselev, and G. A. Pasmanik, "Experimental investigation of the spatial structure of the first Stokes component of stimulated Raman scattering," Sov. J. Quantum Electron. **9**(5), 585–589 (1979).
2. N. Basov, A. Grasiuk, and I. Zubarev, "High power Raman lasers: Beam combining and beam clean up," in *Raman Spectroscopy: Sixty Years On, Vibrational Spectra and Structure*, vol. 17 (Elsevier, 1989), pp. 255–292.
3. J. T. Murray, W. L. Austin, and R. C. Powell, "Intracavity Raman conversion and Raman beam cleanup," Opt. Mater. **11**(4), 353–371 (1999).
4. S. H. Baek and W. B. Roh, "Single-mode Raman fiber laser based on a multimode fiber," Opt. Lett. **29**(2), 153–155 (2004).
5. N. B. Terry, T. G. Alley, and T. H. Russell, "An explanation of SRS beam cleanup in graded-index fibers and the absence of SRS beam cleanup in step-index fibers," Opt. Express **15**(26), 17509–17519 (2007).
6. T. Yao, A. V. Harish, J. K. Sahu, and J. Nilsson, "High-power continuous-wave directly-diode-pumped fiber Raman lasers," Appl. Sci. **5**(4), 1323–1336 (2015).
7. Y. Glick, V. Fromzel, J. Zhang, N. Ter-Gabrielyan, and M. Dubinskii, "High-efficiency, 154 W CW, diode-pumped Raman fiber laser with brightness enhancement," Appl. Opt. **56**(3), B97–B102 (2017).
8. S. A. Babin, A. G. Kuznetsov, O. S. Sidelnikov, A. A. Wolf, I. N. Nemov, S. I. Kablukov, E. V. Podivilov, M. P. Fedoruk, and S. Wabnitz, "Spatio-spectral beam control in multimode diode-pumped Raman fibre lasers via intracavity filtering and Kerr cleaning," Sci. Rep. **11**(1), 21994 (2021).
9. S. A. Babin, E. A. Zlobina, and S. I. Kablukov, "Multimode fiber Raman lasers directly pumped by laser diodes," IEEE J. Sel. Top. Quantum Electron. **24**(3), 1–10 (2017).
10. A. G. Kuznetsov, S. I. Kablukov, E. V. Podivilov, and S. A. Babin, "Brightness enhancement and beam profiles in an LD-pumped graded-index fiber Raman laser," OSA Continuum **4**(3), 1034–1040 (2021).
11. S. A. Babin, A. G. Kuznetsov, O. S. Sidelnikov, S. I. Kablukov, E. V. Podivilov, M. P. Fedoruk, and S. Wabnitz, "Mechanism of brightness enhancement in multimode LD-pumped graded-index fiber Raman lasers," in *Advanced Solid State Lasers*, (Optical Society of America, 2021), pp. JM3A–12.
12. G. P. Agrawal, "Nonlinear fiber optics," in *Nonlinear Science at the Dawn of the 21st Century*, (Springer, 2000), pp. 195–211.
13. K. Krupa, A. Tonello, B. M. Shalaby, M. Fabert, A. Barthélémy, G. Millot, S. Wabnitz, and V. Couderc, "Spatial beam self-cleaning in multimode fibres," Nat. Photonics **11**(4), 237–241 (2017).
14. E. V. Podivilov, D. S. Kharenko, V. Gonta, K. Krupa, O. S. Sidelnikov, S. Turitsyn, M. P. Fedoruk, S. A. Babin, and S. Wabnitz, "Hydrodynamic 2D turbulence and spatial beam condensation in multimode optical fibers," Phys. Rev. Lett. **122**(10), 103902 (2019).
15. W. H. Renninger and F. W. Wise, "Optical solitons in graded-index multimode fibres," Nat. Commun. **4**(1), 1719 (2013).
16. A. Mafi, "Pulse propagation in a short nonlinear graded-index multimode optical fiber," J. Lightwave Technol. **30**(17), 2803–2811 (2012).
17. O. S. Sidelnikov, E. V. Podivilov, M. P. Fedoruk, and S. Wabnitz, "Random mode coupling assists Kerr beam self-cleaning in a graded-index multimode optical fiber," Opt. Fiber Technol. **53**, 101994 (2019).
18. I. S. Chekhovskoy, V. Paasonen, O. Shtyrina, and M. P. Fedoruk, "Numerical approaches to simulation of multi-core fibers," J. Comput. Phys. **334**, 31–44 (2017).

Optics EXPRESS

19. E. A. Evmenova, A. G. Kuznetsov, I. N. Nemov, A. A. Wolf, A. V. Dostovalov, S. I. Kablukov, and S. A. Babin, "2nd-order random lasing in a multimode diode-pumped graded-index fiber," Sci. Rep. **8**(1), 17495 (2018).